Numerical analysis of working fluids for large scale centrifugal compressor driven cascade heat pumps upgrading waste heat

Uusitalo Antti, Turunen-Saaresti Teemu, Honkatukia Juha, Tiainen Jonna, Jaatinen-Värri Ahti

DOI: 10.1016/j.apenergy.2020.115056

Numerical analysis of working fluids for large scale centrifugal compressor driven cascade heat pumps upgrading waste heat

Antti Uusitalo, Teemu Turunen-Saaresti, Juha Honkatukia, Jonna Tiainen, Ahti Jaatinen-Värri

LUT University, School of Energy Systems, P.O. Box 20, 53851 Lappeenranta, Finland

Abstract

Heat pump technology has the capability to upgrade unusable low-temperature waste heat and make the upgraded heat usable for different types of industrial and domestic heating applications. Heat upgrading could allow to reach significant energy savings and reduced emissions when compared to other heat production methods. In this paper, upgrading waste heat into a higher temperature with large-scale centrifugal compressor driven cascade heat pumps was studied numerically. A combined method for heat pump thermodynamic analysis and compressor design analysis was developed and implemented in order to investigate the effect of different working fluid combinations and the effect of the cascade heat exchanger temperature level on the heat pump performance. Seven potential fluid candidates were included and condenser temperature of 90 °C, evaporator temperature of 20 °C, and evaporator heat rate of 1 MW were used in the analysis. It was concluded, that the implemented method can provide an efficient tool for evaluating suitable working fluids and design operating conditions for centrifugal compressor driven high temperature cascade heat pumps. The highest coefficient of performance of 3.08 was simulated by using R601 as the fluid in the low-temperature cycle and R245fa in the high-temperature cycle. These fluids also resulted in feasible compressor geometries and rotational speeds, as well as allowed to reach high compressor efficiencies of well above 80 % based on the enthalpy loss models. Coefficient of performances of over 3.0 were simulated also with the fluid combinations R601/R600, R245fa/R245fa and R600/R245fa.

Keywords: high temperature heat pump, waste heat upgrading, working fluid, centrifugal compressor

Nomenclature

Latin alphabet

P	power	kW
h	enthalpy	kJ/kg
p	pressure	bar
T	temperature	K, ^{o}C
q_m	mass flow rate	kg/s
q_v	volumetric flow rate	m^3/s
D	diameter	m
b	blade height	m
t	tip clearance height	m
n	rotational speed	rpm, 1/s
C	absolute velocity	m/s
U	peripheral velocity	m/s
W	relative velocity	m/s
Z	number of blades	-
q	fluid quality	-
Ma	Mach number	-

Greek alphabet

η	efficiency	-
ϕ	heat rate	kW
Π	pressure ratio	-
ω	angular speed	rad/s
ϵ	wake coverage of flow passage	-
μ	dynamic viscosity	Pa s

Subscripts

1	compressor rotor inlet
2	compressor rotor outlet
avg	average
s	isentropic
cond	condenser
c	compressor
e	electrical
df	disk friction
sf	skin friction
tc	tip clearance
lea	leakage
tip	blade tip
hub	blade hub
rec	recirculation
mix	mixing
r	radial/axial
u	peripheral
sat	saturated
sc	subcooling
sh	superheating
mg	motor and mechanical losses

Abbreviations

CHE	cascade heat exchanger
COP	coefficient of performance
LT	low temperature
HT	high temperature

1. Introduction

One of the most effective ways in reducing emissions and increasing energy efficiency is related to utilizing waste heat that is generated in different types of processes in large quantities [1]. Examples of energy intensive industries with high amounts of low temperature waste heat are e.g. the pulp and paper, cement, steel, glass, textile, and food industry [1] as well as data centers [2]. The majority of industrial waste heat is at low temperatures that often makes the direct utilization of the heat economically and technologically

unattractive [1]. When considering large quantities of industrial waste heat, a significant energy saving potential is evident even if only a small fraction of the heat can be recovered or upgraded into usable form. One of the technologies that has been considered as possible in energy recovery and energy savings, is the implementation of different types of heat pumps. Overall, heat pump technology has faced recent progresses via advanced cycle designs, improved performances and reliability of cycle components, and in recognized utilisation potential in a wide range of different applications [3]. The high temperature heat pump technology, enabling temperature lifts from about 60 ^{o}C to over 100 ^{o}C, could offer high energy savings especially in countries with a cold climate as well as in many industrial sectors having significant need for heating power [4]. According to Averfalk et al. [5] over 1500 MW of heating power with heat pumps was installed in Swedish district heating networks during the 1980s and most of this capacity is still in operation showing that a long technical lifetime can be achieved for large-scale heat pumps. One example of modern heat pump technology for upgrading low grade heat to a district heating network is a facility located in Finland and that has a total heating capacity of 90 MW [6]. Upgraded heat could also be used directly in industrial processes to fulfill the heating demand [4]. In addition, it has been investigated that high temperature heat pumps can be efficiently used in trigeneration systems [7].

The working fluid has a significant impact on heat pump performance and different fluids have been considered and investigated. For a certain application, the optimal fluid depends on operating temperatures and power scales as well as on the component design. In general, the fluids of high temperature heat pumps include different hydrocarbons (e.g. pentane, butane), fluorocarbons (e.g. R134a, R245fa), and rather simple molecule fluids such as ammonia or CO_2 [4]. The use of different fluids has been evolving during the last decades as the use of some fluids has been or will be banned due to their negative environmental impacts [8]. Thus, new types of fluids with zero ozone depleting potential (ODP), and low global warming potential (GWP) have been developed. Other aspects that affect the fluid selection can be considered to be the toxicity, flammability, availability, price and compatibility with materials. In addition, the shape of the saturated vapor curve has an impact on the heat pump design, performance and operational characteristics [9]. For wet and isentropic fluids, only little or no superheating is required at the compressor inlet as the compression remains in the superheated region. When using fluids with an overhanging saturated vapor curve more superheating at the compressor inlet can be required to maintain the compressor outlet in the superheated vapor region [9]. Based on the review by Zhang et al. [10] it was concluded that it is important to study and develope new refrigerants especially for high temperature heat pumps as currently there are not many fluids that are suitable for high temperatures and are environmentally friendly. In a study by Domanski et al. [11], the effect of different fluids on the performance limits of vapor compression cycles was investigated. Different refrigerants and four different cycle layouts were included in their study. It was concluded that the critical temperature of the fluid is the most dominant parameter influencing on the coefficient of performance (COP) and volumetric heating capacity. Zhang et al. [12] investigated the

use of non-zeotropic mixtures of R152a and R245fa in a heat pump with a temperature lift of 45 ^{o}C and condensing temperature of about 90 ^{o}C. They concluded that the use of refrigerant mixtures results in higher COP and higher heating capacity when compared to the use of R245fa. Fukuda et al. [13] studied both experimentally and numerically the use of the low GWP fluids R1234ze(E) and R1234ze(Z) in high temperature heat pumps. They concluded that these fluids can be used in heat pump systems having high condensing temperatures of over 100 ^{o}C and are potential fluids for industrial heat pumps.

With high temperature lifts, the compression work increases when compared to systems operating with lower temperature lift. The high compression work significantly reduces the COP of a heat pump if a simple cycle configuration with a single compressor is used. Thus, in many high temperature heat pumps the compression is divided between two compressors to reduce the compression power consumption [4]. One solution that has been suggested for high temperature lift is the use of cascade heat pumps [3]. In a cascade heat pump there is a low temperature (LT) and high temperature (HT) cycle where the fluids remain unmixed between the cycles and the heat is transferred between the cycles via a cascade heat exchanger (CHE). As the fluids of the two loops remain unmixed, cascade heat pumps can use different fluids in the LT and HT cycle whereas the same fluid has to be used in both the LT and HT loop in a flash intercooled or in some other type of two stage heat pump. Several studies, containing both numerical and experimental research have been carried out for cascade heat pumps. Wang et al. [14] compared the performance of a cascade heat pump and a simple heat pump. They concluded that the energy efficiency ratio was improved by 20 % by using a cascade heat pump. Kim et al. [15] studied the optimal temperature between high and low temperature loops in a cascade heat pump using R134a and R410a as the working fluids. Their numerical and experimental results indicate that the optimal temperature between the two stages is dependent on the ambient conditions, the heating circuit temperature level and the heating power requirement. The dependency between the intermediate temperature level and the above mentioned factors originates from the variations in temperature difference between the condenser and evaporator in different operating conditions. Ma et al. [16] experimentally studied a cascade heat pump for heating water by using a new zeotropic refrigerant mixture BY-3 in the LT cycle and R245fa as the fluid in the HT cycle. They concluded that a very high water outlet temperature of 142 ^{o}C with a condensing temperature of close to 150 ^{o}C and COP of 1.7 could be reached with the studied system. Kim and Kim [17] studied the effect of the temperature lift on the performance of cascade heat pumps. They concluded that a high evaporating temperature leads to high compressor inlet density and increased working fluid flow rate with high water temperature lift. This increases the heating capacity with regard to water temperature lift but decreases the COP. Messineo and Panno [18] investigated the use of different fluids in cascade heat pumps. They used CO_2 as the working fluid in the LT cycle and ammonia, propane, butane, R404A, R410A and R134a as the working fluids in the HT cycle. They suggested that fluids categorized as natural refrigerants show an interesting alternative when compared to the synthetic fluids from an energy, safety and environmental

point of view.

In the majority of the commercial small-scale heat pump systems and experimental facilities, different types of volumetric compressors, including scroll [19], screw [20] or piston [21] compressors have been used instead of kinetic compressors. However, higher compressor efficiencies and improvements in COP could be potentially achieved by using kinetic compressors. Kinetic turbocompressors have already been implemented as the compressor technology especially in some commercial large-scale HT heat pump systems [22]. Turbocompressors have also been considered as the potential technology for increasing the performance in some smaller scale heat pump systems [23]. Along with the increased performance, centrifugal compressor based heat pumps could potentially offer an oil-free solution, which can be considered as a considerable advantage in the design of advanced multistage heat pumps [23]. In the literature, there are only some detailed studies on using centrifugal compressors in heat pumps or in refrigerant cycles. In studies by Schiffmann and Favrat [23] and [24] a small scale centrifugal compressor using R134a as the working fluid was designed and studied experimentally. The investigated compressor impeller had a tip diameter of 20 mm, rotational speed of up to 210 krpm and reached pressure ratios of about 3.3. Despite the small-scale of the investigated compressor a rather high isentropic efficiency of slightly below 80 % was measured. More recently Meroni et al. [25] investigated centrifugal compressor driven heat pumps for generating 150 ^{o}C steam. They concluded that the existing loss correlations for centrifugal compressors can provide rather accurate efficiency predictions in heat pump systems when compared to the experimental data. Their results also indicated that the use of different fluids results in different optimal rotational speed, compressor geometry and efficiency. It has also been concluded in previous studies that centrifugal compressor driven two-stage heat pumps can reach high COP values also when running the system in off-design conditions [26]. Turunen-Saaresti et al. [26] studied the prediction methods and off-design characteristics of a two-stage centrifugal compressor driven refrigeration cycle. They suggested a method to predict the COP in a wide range of different operating conditions by using combined performance map taking into account the off-design characteristics of the both compressors. Röyttä et al. [27] investigated the optimization of a two stage centrifugal compressor driven refrigeration cycle. The investigated fluids were R134a and R245fa. They concluded that in this type of system the optimal operating point is not at the optimum efficiency point of either compressor stage but instead it is a point where both compressors can be operated with a relatively high efficiency.

Based on the literature review, several experimental and numerical studies have been carried out regarding the operation of HT heat pumps. However, the knowledge on how the use of different working fluids and operating parameters affect the performance of high temperature heat pumps seems to be scarce and most of the studies have been concentrated on rather small-scale heat pump systems with the heating capacities ranging from tens of kW to several hundreds of kW [4]. In addition, in the majority of the working fluid selection studies the effects of different fluids and design operating conditions on compressor design and efficiency have been neglected that can lead to non-optimal heat pump designs. Systematic approaches

on predicting how the use of different fluids and the heat pump design conditions affect the compressor geometry, optimal rotational speed and loss distribution seem to be missing in the present literature. In this paper, the performance of a large-scale cascade type heat pump upgrading low-grade waste heat, having a typical temperature range of 30 to 50 ^{o}C, to higher temperature is investigated with different fluids. The evaporator temperature of 20 ^{o}C and the evaporator heat rate of 1 MW were selected for the analysis. The condenser temperature of 90 ^{o}C was selected for the study as this temperature level was evaluated to be sufficient for utilizing the heat in district heating networks or in several other heating applications. The novelty of this work is to investigate the effect of different working fluid combinations and cascade heat exchanger temperature levels on the performance and design parameters of large-scale centrifugal compressor driven heat pumps, by taking into account not only the thermodynamic cycle performance but also investigating the design of compressors and compression losses with different fluids and heat pump design conditions. A method combining the thermodynamic analysis of the heat pump and compressor design as well as a compressor loss analysis method was developed and implemented to identify the most potential working fluid combinations and optimal CHE temperature level. The aim and objectives of the study can be summarized as follows: 1) Which fluid combinations can provide high heat pump performances for the studied temperature level and power level? 2) How does the temperature level in the CHE affect performance with different fluid combinations? 3) How does the different fluid combinations affect the impeller geometry, rotational speed and efficiency prediction of the centrifugal compressors? The results of this study and the presented method can be utilized by engineers and researchers in the future development of high performance large-scale heat pump systems.

2. Methods

In this section, the heat pump layout and calculation methods of the thermodynamic cycle analysis are presented first. Second, the design methods and loss analysis methods for centrifugal compressors are presented.

2.1. Cycle layout and thermodynamic analysis

The studied layout and the main components of the cascade heat pump are presented in Figure 1. An example of the studied heat pump cycle on the log-p,h plane and on the T,s plane are presented in Figure 2a and b.

The system has a LT loop including an evaporator, a LT compressor and a LT expansion valve. The HT loop has a HT compressor, condenser and a HT expansion valve. The heat is transferred between the two loops via a CHE in where the superheating of the LT loop fluid is removed, fluid is condensed and subcooled, whereas the fluid of the HT loop is evaporated and superheated. The thermodynamic state at

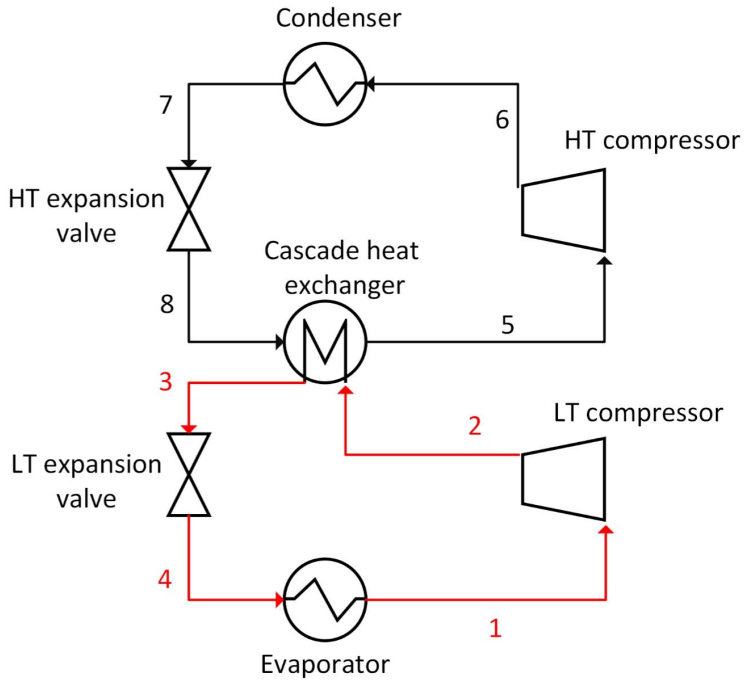

Figure 1: Layout of the investigated two-stage cascade heat pump.

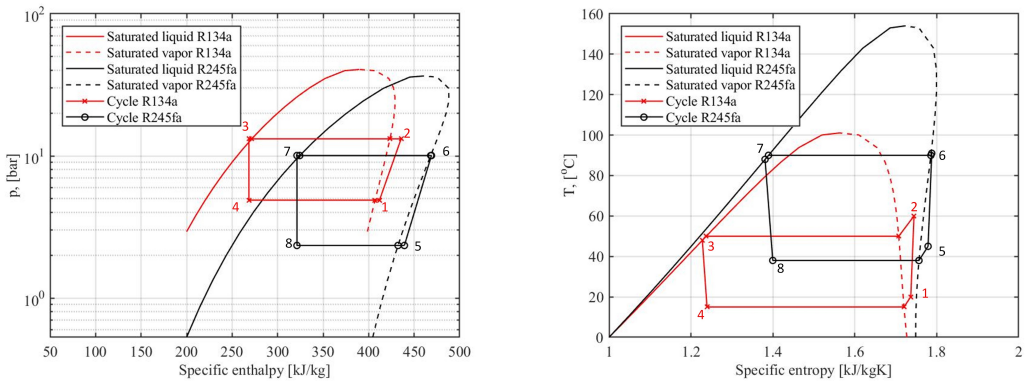

(a) (b)

Figure 2: Example cascade heat pump cycle on the log-p,h plane (a) and on the T,s plane (b). R134a is used in the LT cycle and R245fa in the HT cycle.

different process nodes were defined using the commercial thermodynamic library Refprop [28] that contains high accuracy thermodynamic models for a large number of fluids including different hydrocarbons and refrigerants. The main input parameters for the simulation are presented in Table 1 and the calculation procedure for defining the fluid state at each process node is presented in Table 2. In Table 2, the process nodes are numbered as in Fig.1. The evaporator heat rate of 1 MW was selected for the study, as this

power level was considered to be available in low temperature waste heat streams in a significant number of industrial facilities globally [1]. The evaporation temperature of 20 ^{o}C was selected according to typical industrial low temperature waste heat temperature levels ranging from about 30 to 50 ^{o}C [1] and having insufficient temperature levels to be utilized directly for heating purposes. The temperature level of 90 ^{o}C in the HT loop condenser was evaluated to be sufficient for supplying the heat to district heating networks according to the temperature levels of district heating networks in the Nordic countries [29, 30]. The simulations were performed with LT loop condensing temperatures ranging from 30 ^{o}C to 70 ^{o}C by using 5 ^{o}C steps in order to investigate the effect of the CHE temperature on COP with different fluid combinations. The degree of superheating before the compressors was kept at 5 ^{o}C if the compressor outlet state remained in the superheated vapor region. For fluids with an overhanging saturated curve, especially when using R601, the degree of superheating had to be slightly increased in some simulations in order to maintain the compressor outlet in the superheated vapor region. The change in the degree of superheating also slightly changes the $\Delta\, T$ between the condensing and evaporating fluid in the CHE. The compressor motor efficiency was estimated from the efficiency levels of modern high-speed electric machines [31].

Table 1: Summary of input parameters for the thermodynamic analysis.

Saturated temperature in the HT condenser	90 ^{o}C
Saturated temperature in the LT evaporator	20 ^{o}C
Saturated temperature in the LT condenser	varied from 30 to 70 ^{o}C by using 5 ^{o}C step
ΔT between the condensing and evaporating fluid in CHE	10 ^{o}C
Degree of subcooling	3 ^{o}C
Degree of superheating before the compressors	min. 5 ^{o}C
Compressor mechanical and electrical efficiency	90 %

In the thermodynamic analysis, heat pump calculation principles based on solving the fluid thermodynamic state at different process nodes and solving the energy balance and continuity equation for each process component were followed. Pressure and heat losses in the components and in piping were excluded. By assuming a maximum pressure drop of 0.5 bar for each heat exchanger, the effect of pressure losses on heat pump COP was estimated to be in the order of magnitude of 2 % to 7 % depending on the working fluid combination. The working fluid flow rate in the LT cycle was solved as

$$q_{\mathrm{m,wf,LT}} = \frac{\phi_{\mathrm{ev}}}{(h_1 - h_4)}. \tag{1}$$

The heat power of the CHE was solved as

Table 2: Calculation procedure for the thermodynamic analysis.

node	inputs	solved with Refprop [28]
1	p,T=($T_{2-3'}$+ΔT_{sh})	h,s,ρ,μ,q
2	h,p=($p_{2-3'}$)	T,s,ρ,μ,q
2-3' (saturated vapor in the CHE LT loop)	T,q	p,h,s,ρ,μ
2-3" (saturated liquid in the CHE LT loop)	$T = T_{2-3''}$,q	p,h,s,ρ,μ
3	$T = T_{2-3''}$ -ΔT_{sc}, p	h,s,ρ,μ,q
4	p, h (=h_3)	T,s,ρ,μ,q
4-1' (Saturated vapor in the evaporator)	p,q	T,h,s,ρ,μ
5	p,T	h,s,ρ,μ,q
6	h,p=($p_{6-7'}$)	T,s,ρ,μ,q
6-7' (Saturated vapor in the condenser)	T,q	p,h,s,ρ,μ
6-7" (Saturated liquid in the condenser)	$T = T_{6-7''}$, q	p,h,s,ρ,μ
7	$T = T_{6-7''}$ -ΔT_{sc},p	h,s,ρ,μ,q
8	p, h (=h_7)	T,s,ρ,μ,q
8-5' (Saturated vapor in the CHE HT loop)	p,q	T,h,s,ρ,μ

$$\phi_{\mathrm{CHE}} = q_{\mathrm{m,wf,LT}}(h_2 - h_3). \tag{2}$$

From the energy balance of the CHE, the fluid mass flow rate in the HT loop was solved as

$$q_{\mathrm{m,wf,HT}} = \frac{\phi_{\mathrm{CHE}}}{(h_5 - h_8)}. \tag{3}$$

The condenser heat rate was solved as

$$\phi_{\mathrm{cond}} = q_{\mathrm{m,wf,HT}}(h_6 - h_7). \tag{4}$$

The enthalpies at the compressor outlets (node 2 and 6) were solved from the definition of isentropic efficiency when the compressor inlet state and outlet pressure are known as

$$h_{\mathrm{c,out}} = h_{\mathrm{c,in}} + \frac{(h_{\mathrm{c,out,s}} - h_{\mathrm{c,in}})}{\eta_{c,s}}. \tag{5}$$

in which $h_{\mathrm{c,out,s}}$ was solved based on the isentropic compression from the compressor inlet state to the compressor outlet pressure.

The fluid power of the LT and HT compressors was calculated as

$$P_{\mathrm{c}} = q_{\mathrm{m,wf}}(h_{\mathrm{c,out}} - h_{\mathrm{c,in}}). \tag{6}$$

The electric power consumption of the LT and HT compressors was calculated as

$$P_{\mathrm{e}} = \frac{P_{\mathrm{c}}}{\eta_{mg}}. \tag{7}$$

The coefficient of performance for the heat pump was calculated as

$$COP = \frac{\phi_{\mathrm{cond}}}{P_{\mathrm{e,LT}} + P_{\mathrm{e,HT}}}. \tag{8}$$

2.1.1. Cycle analysis code validation

The heat pump cycle analysis code was validated against the results presented by Wang et al. [32] for a cascade heat pump using R502 in the LT cycle and R152a in the HT cycle. In the analysis R502 was modelled as a mixture of R22 and R115 with the mass fractions of 48.8 % and 51.2 %[28]. The LT cycle evaporation temperature, the HT cycle condensing temperature as well as the saturated temperatures in the CHE were set to the same values as were given in [32]. Isentropic efficiencies of both the compressors were set to 80 % and the LT evaporator heat rate was set to 144.65 kW as in the analysis by Wang et al. [32]. The comparison of the heat pump temperatures and pressures obtained from the heat pump analysis code and presented in [32] is presented in Table 3. The comparison of the calculated compressor and heat powers are presented in Table 4. In general, the comparison shows that the developed model and the results presented by Wang et al. [32] have a relatively good agreement in the component power levels as well as in process pressure and temperature levels. The highest deviations in temperatures between the model and the results of Wang et al. [32] were observed at the outlets of the compressors and especially in the LT cycle. Overall, the relative differences in the calculated component powers were in the order of magnitude of 2% or less and the differences in the process pressure levels were almost negligible.

2.2. Compressor design

The centrifugal compressor design was based on solving the velocity triangles and main dimensions by following the guidelines available in the literature. The design guidelines of Japikse [33], Balje [34] and Came and Robinson [35] were followed. An example of a compressor impeller is shown in Figure 3a showing the solved dimensions. A schematic drawing of velocity triangles at the impeller inlet and outlet are presented in Figure 3b. The compressor optimal rotational speed was calculated to reach the specific speed of $N_s = 0.8$ that generally allows to reach a high efficiency for a centrifugal compressor [34]. The velocity ratios C_{u2}/U_2 and C_{r2}/U_2 were selected to reach a suitable flow angle and velocity triangle shape at the compressor outlet [34, 35].

Table 3: Comparison of cycle temperatures and pressures.

node	T_{ref}, [K] [32]	T_{calc}, [K]	p_{ref}, [bar] [32]	p_{calc}, [bar]
1	256	256	3.2	3.2
2s	312.8	308.5	13.7	13.5
2	320.1	315	13.7	13.5
2-3'	305	305	13.7	13.5
2-3"	305	305	13.7	13.5
4	256	255.9	3.2	3.2
5	300	300	6.3	6.3
6s	347.2	352.3	18.4	18.4
6	357.2	357.6	18.4	18.4
6-7'	342	342	18.4	18.4
6-7"	342	342	18.4	18.4
8	300	300	6.3	6.3

Table 4: Comparison of the component powers.

Component	[32]	calculated
ϕ_{cond}, kW	239.5	235.2
ϕ_{CHE}, kW	192.4	192.1
$P_{\mathrm{c,LT}}$, kW	46.8	47.5
$P_{\mathrm{c,HT}}$, kW	44.1	43.1

The suitable compressor rotational speed was solved from the specific speed defined as

$$N_s = \frac{\omega {q_{v1}}^{0.5}}{{\Delta h_s}^{0.75}}. \tag{9}$$

By using the Euler turbomachinery equation and by assuming the flow entering the compressor wheel in axial direction without any preswirl ($C_{\mathrm{u1}} = 0$) at the design condition, the peripheral velocity U_2 was solved as

$$U_2 = \frac{\Delta h_c}{C_{u2}}. \tag{10}$$

Once the U_2 and n are solved, the compressor wheel outlet diameter was solved as

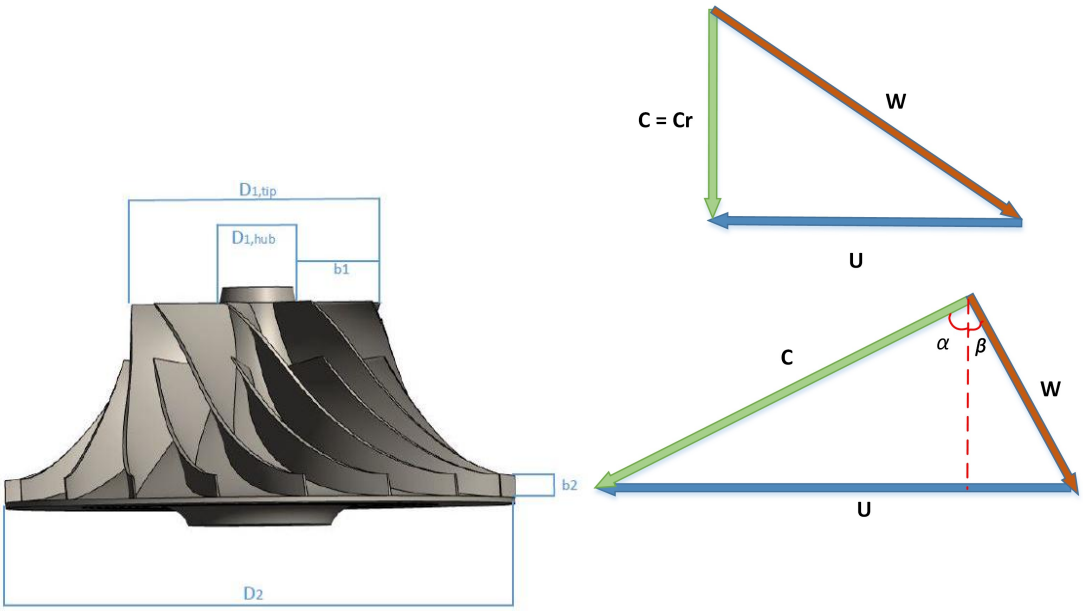

(a) (b)

Figure 3: (a) Example of a centrifugal compressor impeller with every second blade being a full blade and every second a splitter blade and (b) schematic drawing of the velocity triangles at the impeller inlet and outlet.

$$D_2 = \frac{U_2}{\pi n}. \tag{11}$$

The rotor inlet blade height and outlet blade height was calculated by using the continuity equation and the velocity triangles at the compressor inlet and outlet. The rotor diameter and blade height at the rotor inlet are calculated by using the diameter ratios $D_{1,\text{tip}}/D_2$ and $D_{1,\text{hub}}/D_{1,\text{tip}}$.

On the evaluation of compressor losses, enthalpy loss models were implemented for different loss sources. The studied losses were disk friction, tip clearance, skin friction, blade loading, leakage, recirculation and mixing loss. These loss models were selected according to suggestions by Oh et al. [36] about the optimal set of loss correlations for centrifugal compressors. In addition, correlations of similar types have been used for estimating losses in centrifugal compressors operating with real gases, including refrigerants [24] and supercritical CO_2 [37, 38]. In a recent study by Meroni et al. [25] heat pump compressor efficiency prediction at both design and off-design conditions based on loss correlations were compared to measured compressor cases showing good agreement between the results of the measurements and the models. In their study, most of the implemented loss correlations were the same as the ones applied in this study.

The incidence loss caused by the misalignment of the blade with respect to the flow was considered

negligible when running the compressor close to the design conditions. The disk friction loss was evaluated by using the model from Daily and Nece [39] and was defined as

$$\Delta h_{df} = 0.5f(\rho_1 + \rho_2)D_1^2 \frac{U_2^3}{16 q_{m,wf}} \tag{12}$$

in where

$$Re = \rho_2 U_2 \frac{D_2}{2\mu_2} \tag{13}$$

$$f = \frac{0.0622}{Re^{0.2}}. \tag{14}$$

The tip clearance loss is a loss caused by the flow leaking from the pressure side of the blade to the suction side through a gap between the impeller and the casing. The tip clearance loss was evaluated by using the model from Jansen [40] and is defined as

$$\Delta h_{tc} = 0.6 \frac{t}{b_2} C_{u2} \sqrt{2 \frac{\pi}{V_d V_n} C_{u2} C_{r1} \frac{D_{1,tip}^2 - D_{1,hub}^2}{(D_2 - D_{1,tip})(1 + \frac{\rho_2}{\rho_1})}}. \tag{15}$$

The skin friction loss is a loss originating from enthalpy rise caused by the friction on the impeller surfaces. The skin friction loss was evaluated by using the model from Jansen [40]

$$\Delta h_{sf} = 2C_f \frac{L_b}{D_{hyd}} \overline{W}^2 \tag{16}$$

in where $C_f = 0.006$ was selected according to the suggested value by Jansen [40] and

$$L_b = \frac{D_{1,tip}}{2} + D_2 - D_{1,hub} \tag{17}$$

$$D_{hyd} = \pi \frac{D_{1,tip}^2 - D_{1,hub}^2}{\pi D_{1,tip} + 2Z(D_{1,tip} - D_{1,hub})} \tag{18}$$

$$\overline{W} = \frac{2W_2 + W_{1,tip} + W_{1,hub}}{4}. \tag{19}$$

The blade loading loss is caused by the fluid momentum loss originating from the boundary layers on the blade surfaces. The loss was evaluated by using the correlation by Coppage et al. [41] and is defined as

$$\Delta h_{bl} = 0.05 D_f^2 U_2^2 \tag{20}$$

in where the diffusion factor is

$$D_f = 1 - \frac{W_2}{W_{1,tip}} + \frac{0.75((U_2 C_{u2} - U_1 C_{u1})/U_2^2}{\frac{W_{1,tip}}{W_2}[Z/\pi(1 - D_{1,tip}/D_2) + 2(D_{1,tip}/D_2)]} \tag{21}$$

Leakage loss represents the loss when flow through the clearance gap re-enters the blade passage and mixes with the main flow. The leakage loss was estimated by using the correlation by Aungier [42]

$$\Delta h_{lea} = \frac{q_{mcl} U_{cl} U_2}{2 q_m} \tag{22}$$

where

$$q_{mcl} = \rho_2 Z t L_b U_{cl} \tag{23}$$

$$U_{cl} = 0.816 \sqrt{\frac{2\Delta P_{cl}}{\rho_2}} \tag{24}$$

$$\Delta P_{cl} = \frac{q_m (D_2 C_{u2} - D_{1,tip} C_{u1})}{2 b_{avg} \overline{r} \overline{b} L_b} \tag{25}$$

$$\overline{b} = \frac{D_{1,tip} - D_{1,hub} + b_{avg}}{2} \tag{26}$$

$$\overline{r} = \frac{D_2 + D_{1,tip}}{4}. \tag{27}$$

The recirculation loss, caused by the low momentum fluid recirculating from the vaneless space back into the impeller passage was defined by using the correlation from Oh and Chung[43]

$$\Delta h_{rec} = 8.0 * 10^{-5} sinh(3.5\alpha_2) * D_f^2 * U_2^2. \tag{28}$$

Mixing loss originating from the non-uniform velocity profile at the impeller outlet was defined by using the model from Johnston and Dean [44]

$$\Delta h_{mix} = (\frac{C_2}{cos\alpha_2})^2 (\frac{(1-\epsilon) - b^*}{1-\epsilon})^2 \tag{29}$$

where the ϵ is the dimensionless fraction of blade-to-blade space occupied by the wake and b^* is the diffuser inlet to impeller outlet blade height ratio.

The total loss was calculated as

$$\Delta h_{loss} = \Delta h_{df} + \Delta h_{tc} + \Delta h_{sf} + \Delta h_{bl} + \Delta h_{lea} + \Delta h_{rec} + \Delta h_{mix} \tag{30}$$

and the efficiency was defined as

$$\eta_c = \frac{\Delta h_s}{\Delta h_s + \Delta h_{loss}}. \tag{31}$$

Table 5: Summary of input parameters for compressor design.

Z	18
Blade thickness	2 mm
t	0.5 mm
$D_{1\mathrm{tip}}/D_2$	0.5
$D_{1\mathrm{hub}}/D_{1\mathrm{tip}}$	0.3
N_s	0.8
$C_{\mathrm{u}2}/U_2$	0.65
$C_{\mathrm{r}2}/U_2$	0.3

The possible losses in the volute and diffuser were not taken into account in defining the compressor losses in this study. A summary of input parameters used in the compressor design is presented in Table 5.

As a result, the compressor inlet and outlet diameters, blade heights, rotational speed, as well as the isentropic efficiency can be evaluated for different heat pump designs. The compressor efficiency estimation was updated to the thermodynamic analysis tool and the calculation was iterated until there were no significant changes in the geometry and efficiency (relative efficiency change between the iterations $<$ 1e-5 %). A similar approach combining turbomachinery design and cycle thermodynamic analysis has been recently used for supercritical Brayton cycles [45]. The calculation procedure combining the cycle calculation and the compressor design, as well as the model inputs and outputs is presented in Fig. 4.

2.2.1. Compressor design code validation

Well documented centrifugal compressor designs with sufficient geometry information and efficiency predictions were selected as the validation cases for the compressor design code. The first compressor uses air as the working fluid, has a pressure ratio of 2.5, flow rate of 1.8 kg/s and rotational speed of 27660 rpm. The working fluid flow rate, the compressor inlet temperature and pressure, the compressor outlet pressure, the rotational speed, the shape of the velocity triangle at the rotor outlet ($C_{\mathrm{r}2}/U_2$, $C_{\mathrm{u}2}/U_2$), the diameter ratios ($D_{1,\mathrm{tip}}/D_2$, $D_{1,\mathrm{hub}}/D_2$), the number of blades, and the tip clearance height were set to the same values as in [46]. The results of the compressor design code as well as the geometry and efficiency information [46, 47] are compared in Table 6. The model predicted isentropic efficiency of 83.3 %, whereas the CFD based efficiencies in [46] varied from 81 to 90 % depending on the implemented turbulence model. In the experimental study, an efficiency of about 80 % was recently measured [47].

The second compressor used for the code validation is a small scale compressor using R134a as the working fluid[23, 24]. The compressor is designed to operate at pressure ratios ranging from about 1.7 to 4.2

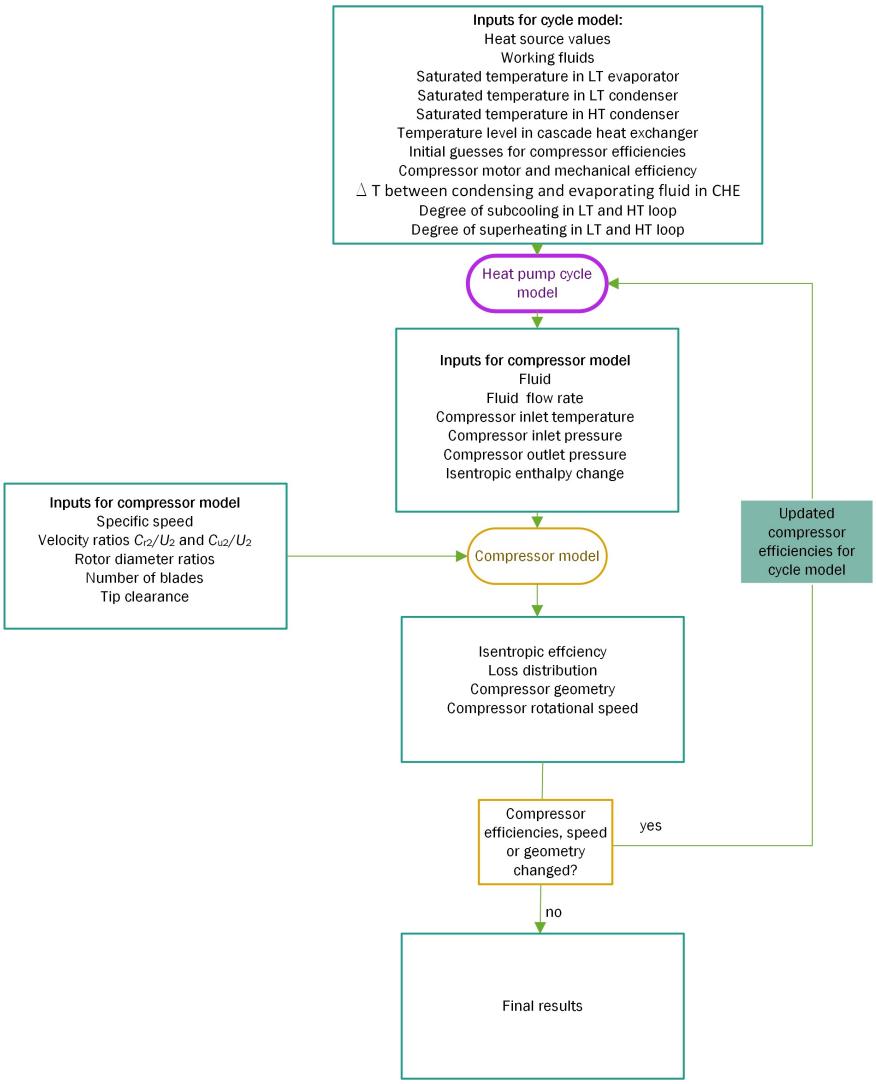

Figure 4: Calculation procedure for combining the thermodynamic analysis and design of centrifugal compressors.

with compressor rotational speeds ranging from 150 to 200 krpm[24], and it has 18 blades. A pressure ratio of 3.3, a rotational speed of 210000 rpm and a mass flow rate of 0.04 kg/s were selected for the compressor design as the design conditions. In addition, the diameter ratios $D_{1,\mathrm{tip}}/D_2$ of 0.57 and $D_{1,\mathrm{hub}}/D_2$ of 0.35, blade thickness of 2 mm, and tip clearance of 0.1 mm were selected for the compressor design as input values. The compressor design code predicted an efficiency of 82.7 % for the R134a compressor whereas in [24] it is mentioned that an efficiency of 84 % was predicted by using CFD analysis and compressor efficencies

slightly below 80 % were measured[24].

The input values are summarized and the results of the developed compressor design code as well as the geometry information of the compressors for the code validation are compared in Table 6. Overall, the developed compressor design model results in compressor main dimensions with only minor differences to the dimensions of the compared compressor designs. The most notable deviation was in the air driven impeller outlet blade height, whereas the differences in the compressor diameters are almost negligible. In addition, the predicted isentropic efficiency is close to the ones predicted with CFD and defined by measurements in the studies of Naukkarinen [46] and Dewar et al. [47] and in the study of Schiffman and Favrat [24] that brings confidence that the applied loss correlations can provide a rather accurate efficiency predictions for different centrifugal compressor designs.

Table 6: Input values and comparison of the compressor design code results to compressor dimensions and performances available in the literature. The results of the compressor design code are given in bold in the table.

	fluid	P_c	Π	n	q_m	D_2	$D_{1,tip}$	$D_{1,hub}$	b_2	η (CFD/Meas.)
		kW	-	rpm	kg/s	mm	mm	mm	mm	-
Compressor 1[46, 47]	air	190.0	2.5	27660	1.8	270.9	134.9	40.5	12.16	0.81-0.9/0.8
Compressor design code	air	193.7	2.5	27660	1.8	**270.7**	**135.4**	**40.6**	**10.1**	**0.833**
Compressor 2[24, 23, 25]	R134a	-	3.3	210000	0.04	20.0	11.2	4.0	1.2	0.84/0.8
Compressor design code	R134a	1.4	3.3	210000	0.04	**20.1**	**11.4**	**4.0**	**1.2**	**0.827**

2.3. Studied working fluids

Seven working fluids were selected for the study, namely, R245fa, R717, R134a, R1234yf, R1234ze, R600, and R601. The fluids that were investigated were selected from the fluids that have been recently used or considered to be used for different types of high temperature heat pumps [4]. Some of the fluids that were mentioned in [4] were not considered if they were recognized inappropriate for the studied heat pump in the preliminary screening of the fluids by the authors or if the thermodynamic properties in [28] were not sufficient to conduct the simulations. The summary and the main properties of the studied fluids are presented in Table 7. Each fluid has been studied both in the LT and HT loop in such a way that all the possible combinations were simulated. As the simulations were performed for all the possible fluid combinations and for nine different CHE temperatures, a total of 441 simulation cases were investigated.

3. Results

In this section, the results with different fluid combinations are presented first, secondly the fluid combination that results in the highest COP is analyzed in more detail and thirdly, the effect of CHE temperature

Table 7: Studied working fluids. Data collected from [13, 8, 28, 4].

	Fluid	Molecular formula	M [kg/kmol]	T_{crit} [K]	p_{crit} [bar]	GWP -	p_{sat} (20 ^{o}C) [bar]	p_{sat} (90 ^{o}C) [bar]
R245fa	Pentafluoropropane	$C_3H_3F_5$	134.05	427.16	36.15	858	1.2	4.7
R717	Ammonia	NH_3	17.03	405.4	113.33	< 1	8.6	51.2
R134a	Tetrafluoroethane	CH_2FCF_3	103.03	374.21	40.59	1300	5.7	32.4
R1234yf	2,3,3,3,-tetrafluoropropene	$C_3H_2F_4$	114.04	367.85	33.82	< 4.4	5.9	30.8
R1234ze	trans-1,3,3,3-tetrafluoropropene	$C_3H_2F_4$	114.04	382.52	36.36	6	4.3	24.8
R600	n-butane	C_4H_{10}	58.12	425.13	37.96	≈ 4	2.1	12.5
R601	n-pentane	C_5H_{12}	74.15	469.7	33.7	≈ 5	0.6	4.7

on the Mach number at the outlets of the compressors is investigated.

3.1. Results with different fluid combinations

Table 8 shows the highest simulated COP value for each studied fluid combination. In Table 8, the horizontal row shows the fluid that was used in the LT loop and the vertical row on the left shows the fluid that was used in the HT loop. The maximum COP values that were reached with the different fluid combinations range from 2.47 to 3.08. The COP values of over 3 were simulated with the following fluid combinations: R245fa/R245fa, R600/R245fa, R601/R245fa, R245fa/R600, R601/R600, R601/R601, where the fluid that has been used in the LT loop is mentioned first and the fluid used in the HT loop is mentioned second. R601/R245fa reached the highest COP of the studied combinations. The lowest COPs were simulated with the fluid combinations R717/R1234yf, R134a/R1234yf, R1234ze/R1234yf and R1234yf/R1234yf. It can be observed that the fluids with the highest critical temperatures, namely R245fa, R600, and R601, reached the highest maximum COP values, whereas the use of fluids with the lowest critical temperatures, namely R134a, R1234yf, R1234ze resulted in the lowest maximum COP values, especially when these fluids were adopted in the HT loop. The use of R717 resulted in slightly lower COPs when compared to R245fa, R600, and R601. The simulated maximum COPs of close to 3 agree well or are slightly higher than the performance values given by Arpagaus et al. [4] for the state of the art heat pumps operating with about a 70 ^{o}C temperature lift. The log p,h chart and T,s chart of the case that resulted in the highest performance is presented in Figure 5a and b. It can be noticed that the compression process of both of the compressors occurs close to the saturated vapor curves and thus, only a small amount of desuperheating is required in the CHE and in the HT condenser. The HT loop using R245fa as the working fluid operates with higher pressure levels throughout the cycle when compared to the pressure levels of the LT cycle.

Table 8: Maximum COP values with different working fluid combinations. The horizontal row shows the fluids that are used in the LT loop and the vertical row shows the fluids that are used in the HT loop. The cases with the highest COPs (COP≥3) are in bold.

	R245fa	R717	R134a	R1234yf	R1234ze	R600	R601
R245fa	**3.03**	2.88	2.91	2.87	2.93	**3.01**	**3.08**
R717	2.88	2.74	2.76	2.72	2.77	2.86	2.93
R134a	2.79	2.64	2.64	2.59	2.66	2.77	2.85
R1234yf	2.69	2.55	2.53	2.47	2.55	2.67	2.74
R1234ze	2.85	2.70	2.70	2.65	2.72	2.82	2.91
R600	**3.00**	2.85	2.88	2.85	2.90	2.98	**3.05**
R601	2.94	2.78	2.80	2.75	2.82	2.92	**3.01**

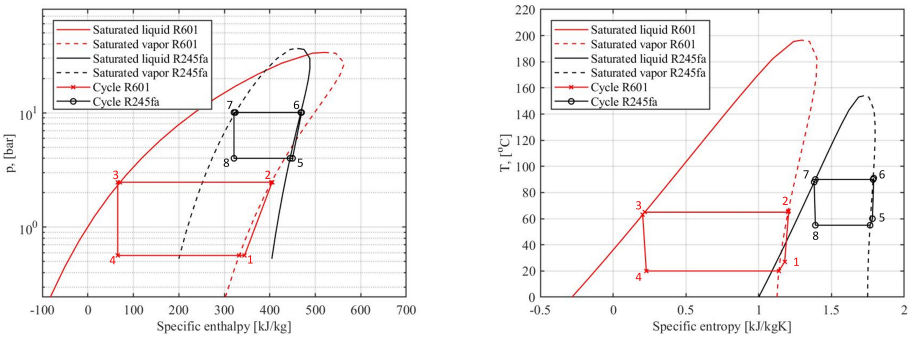

(a) (b)

Figure 5: log,p-h chart (a) and T-s chart (b) of the case with highest COP.

In Figures 6a-d, the effect of LT condensing temperature on COP values has been presented. The results are presented for cases where R245fa has been used in the HT loop in Figure 6a, R717 in Figure 6b, R600 in Figure 6c, and R601 in Figure 6d. For each fluid combination an optimum LT condensing temperature that maximizes the COP was observed. This is the point where the total compressor power is the lowest of the studied conditions and the maximum COPs were reached with rather high LT loop condensing temperatures ranging from 55 to 70 ^{o}C with all the studied cases. It was also observed that when the fluids with the lowest critical temperatures, namely R1234yf, R1234ze and R134a were used in the LT cycle, the maximum COP was generally found at lower LT loop condensing temperature when compared to fluids with higher critical temperatures.

With most of the fluids, the predicted compressor efficiencies were relatively high, ranging from 81 % to

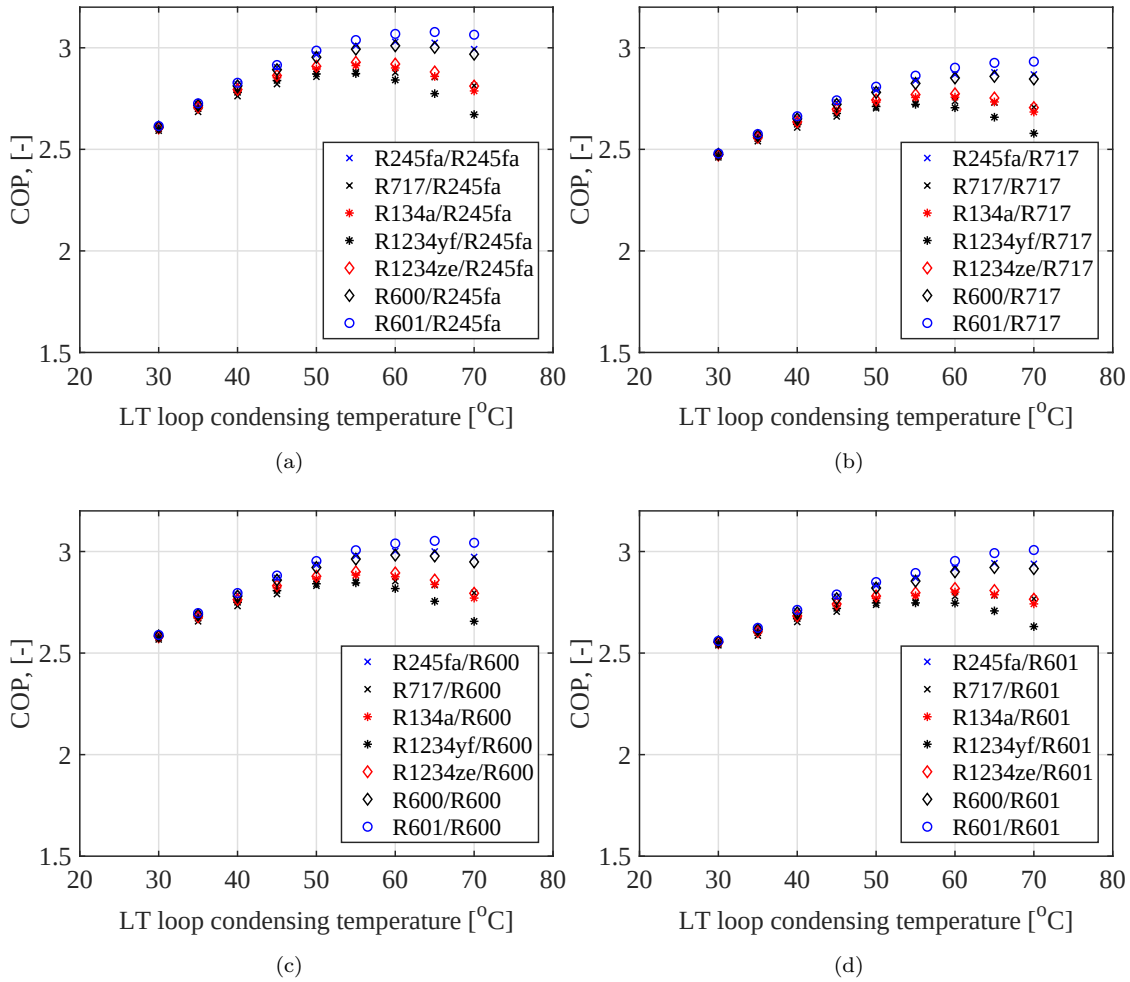

Figure 6: Effect of CHE temperature on COP. R245fa has been used as the HT loop fluid in (a), R717 in (b), R600 (c), and R601 in (d).

84 % in the points where the maximum heat pump COP was reached. Most of the studied fluids resulted in compressor designs with compressor rotational speeds ranging from 15 krpm to 30 krpm and outlet diameters ranging from 150 to 350 mm at the points with the maximum COP. These can be considered technically feasible values for centrifugal compressors as these values are in the same order of magnitude as the values given in [46, 47]. The lower COP with R717 when compared to R245fa, R600, and R601 was caused by the low compressor efficiencies ranging from 70 % to 74 %. The low efficiency mainly originates from the low mass flow rate and high enthalpy change resulting in a small-sized compressor wheel and a significantly high rotational speed requirement to reach the optimal specific speed. The high rotational speed and small dimensions make the design of high efficiency compressors with R717 challenging for the studied power scale due to the significantly high relative tip clearance and leakage losses. For each fluid combination the LT

loop condensing temperature, the power consumption of the compressors, the pressure ratio of the LT and HT cycle, as well as the compressor efficiencies, outlet diameters and rotational speeds corresponding to the heat pump design values with maximum COP are presented in the *Appendix*.

3.2. Detailed analysis of R601/R245fa cycle

In the following, the effect of the LT loop condensing temperature on the compressor design is analyzed in detail for the fluid combination that resulted in the highest COP. R601 is used as the working fluid in the LT loop and R245fa in the HT loop. The effect of CHE temperature on compressor power excluding the motor and mechanical losses is presented in Figure 7a, on compressor efficiency in Figure 7b and on compressor pressure ratio in Figure 7c. The maximum COP was achieved in the design point that is not a point of highest efficiency of either the compressors, but instead it is a point where both of the compressors can be designed to operate at a reasonably high efficiency. The CHE temperature that maximises the heat pump performance is the point where the total compression power consumption is predicted to be the lowest. When the heat pump system is designed for high CHE temperature the power requirement of the LT loop compressor is high and the power consumption of the HT compressor is low. With the low CHE temperatures the LT compressor pressure ratio is low, and consequently the LT compressor power consumption is low, whereas the power consumption and pressure ratio over the HT compressor is increased as the CHE temperature is decreased. As the compressor pressure ratio increases the efficiency decreases. Thus, the optimum CHE temperature that maximizes the COP can be found in such conditions where the pressure ratio over both compressors remains moderate and allows reaching a relatively high isentropic efficiency for both compressors.

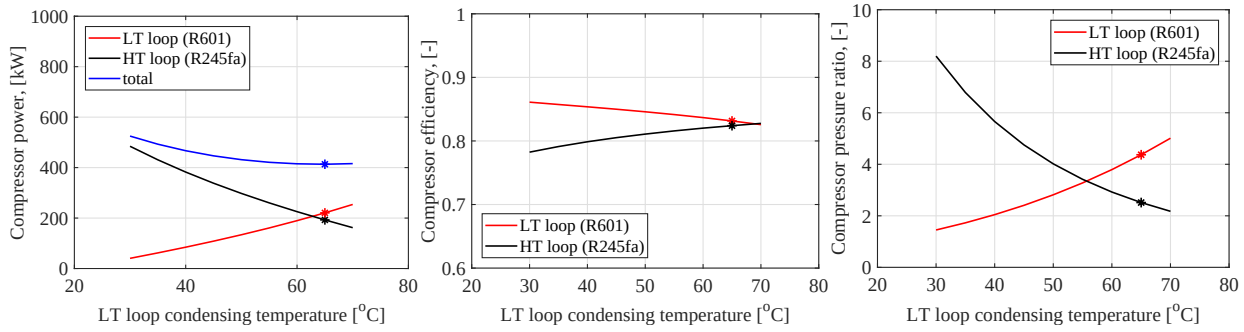

Figure 7: Effect of CHE temperature on (a) compressor power consumption, (b) compressor efficiency, (c) compressor pressure ratio. The markers represent the heat pump design condition with the highest COP.

The effect of the CHE temperature on the optimal design rotational speed of the LT and HT compressors is presented in Figure 8a, on compressor diameters in Figure 8b and on compressor outlet blade heights in

Figure 8c. As the CHE temperature is increased the optimal rotational speed of the LT compressor increases but it does not have a significant effect on the HT compressor optimal rotational speed. The optimal diameter of both the LT and HT compressor decreases as the design CHE temperature increases. The compressor outlet blade height of the HT compressor increases and the outlet blade height of LT compressor decreases as the CHE temperature increases. The changes in the optimal compressor rotational speed, diameter, and blade height originate from the variations in flow rates, enthalpy change over the compressors as well as fluid density changes with different CHE design temperatures.

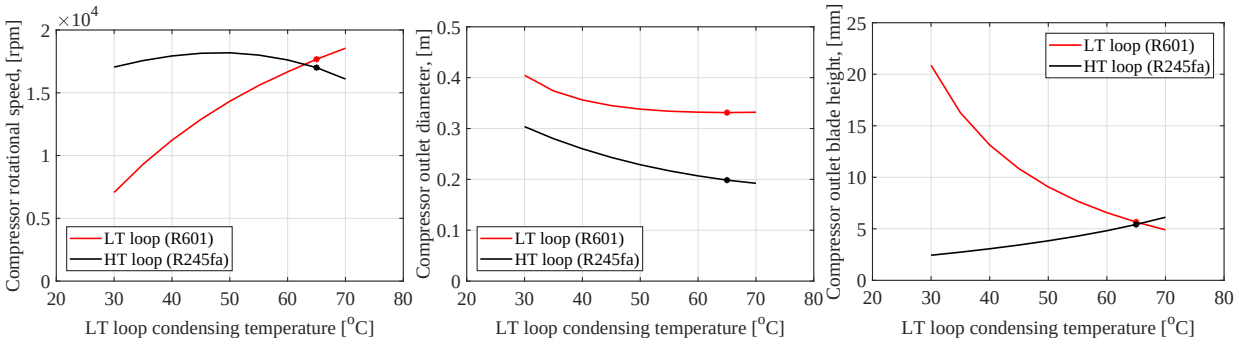

Figure 8: Effect of CHE temperature on (a) compressor design rotational speed, (b) compressor outlet diameter, and (c) compressor outlet blade height.

The effect of the CHE temperature on fluid mass flow rate in the LT and the HT loop is presented in Figure 9a, on enthalpy change over the compressors in Figure 9b and on peripheral speed in Figure 9c. As the design CHE temperature increases, the mass flow rate in the LT loop increases and in the HT loop decreases. The mass flow rate of R245fa in the HT loop is significantly higher than the flow rate of R601 in the LT loop due to the significantly lower enthalpy change of R245fa in the CHE when compared to the enthalpy change of R601 in the CHE. As the system is designed for higher CHE temperature, the enthalpy change over the compressor and the peripheral speed increases in the LT loop and decreases in the HT loop when compared to a system designed for low CHE temperature level. This is due to the differences in the pressure ratios over the compressors when comparing different design cases with different CHE temperature levels.

The effect of CHE temperature level on compressor loss distribution is presented in Figure 10a for the LT compressor and Figure 10b for the HT compressor. The most significant loss sources predicted by the enthalpy loss models are the tip clearance loss and skin friction loss. The skin friction loss decreases in the LT compressor and increases in the HT compressor if the heat pump is designed for high CHE temperature when compared to lower CHE temperatures. This can be explained by the changes in the blade surface

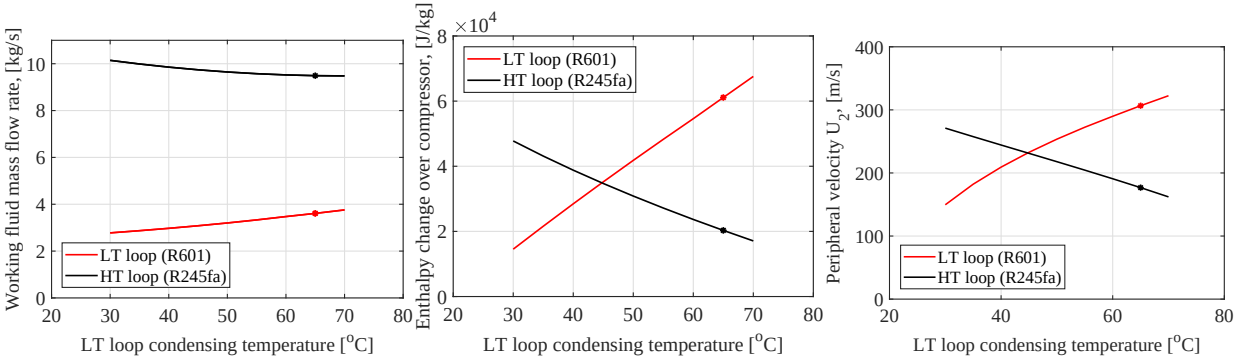

Figure 9: Effect of CHE temperature on (a) mass flow rate, (b) enthalpy change over compressor, and (c) peripheral velocity U_2.

areas and changes in the average relative velocity when comparing different designs. The tip clearance loss of the LT compressor increases and in the HT compressor decreases if the heat pump is designed for high CHE temperature when compared to lower CHE temperature at the design point. This can be explained by the fact that the compressor outlet blade height increases in the HT loop and decreases in the LT loop as the design CHE temperature is increased, and this changes the relative height of the tip clearance gap. The blade loading and leakage loss were also evaluated to have a notable contribution on the total losses of the compressor. The other investigated losses make only a small contribution to the total losses. In [38] the skin friction, tip clearance and leakage loss were also evaluated to be the most significant loss mechanisms in a centrifugal compressor compressing CO_2, whereas the contribution of recirculation and mixing loss was evaluated to be rather small.

3.3. Effect of CHE temperature on compressor outlet Mach number

It was observed in the compressor design that the studied fluids have rather low speed of sound. Thus, the flow can become supersonic despite the velocities remaining moderate, especially when compared to typical velocities in air compressors. High Mach numbers were observed especially at the compressor wheel outlet whereas the velocities can remain as subsonic at the compressor inlet meanline both in absolute and relative frame. The effect of the CHE temperature on the Mach number (Ma) at the outlets of the LT and HT compressor rotors with different fluids is presented in Figure 11a and Figure 11b. As the CHE temperature increases the Ma of the LT compressor increases and the Ma of the HT compressor decreases. This can be explained by the fact that with a low CHE temperature the pressure ratio in the HT cycle is high and the LT cycle is low resulting in requirements for high velocities in the HT compressor and low velocities in the LT compressor. As the LT compressor pressure ratio increases and the HT compressor

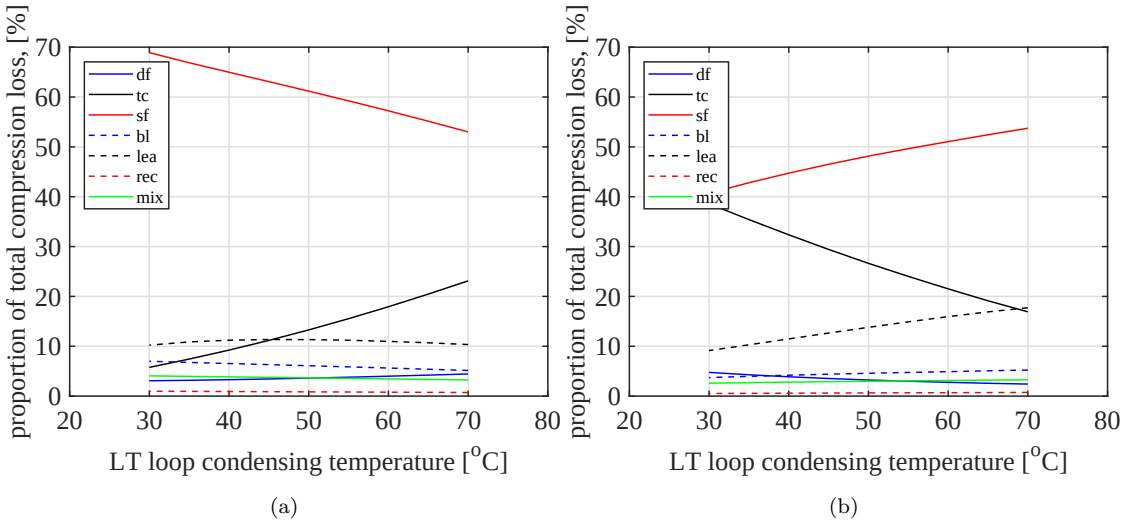

Figure 10: Effect of CHE temperature on predicted (a) LT compressor and (b) HT compressor loss distribution.

decreases, the flow velocities increase in the LT compressor and decrease in the HT compressor. Especially when low CHE temperature is selected, the Ma of the HT compressor becomes significantly high. Thus, it is suggested that with most of the investigated fluid combinations the outlet Ma of both compressors remains at a reasonable level when a CHE temperature level between 50 ^{o}C to 65 ^{o}C is selected. The lowest Mach numbers were observed both in the LT and HT compressors with R717 and the highest ones in the LT compressor with R245fa and in the HT compressor with R601 and R600. If considering only the simulation cases where the outlet velocity of both compressors is limited to be subsonic (Ma $<$ 1), the combination of R601/R1234ze reaches the highest COP of 2.91 with an LT cycle condensing temperature of 70 ^{o}C. In the compressor loss analysis, the losses related to Mach number were neglected and thus, the predicted compressor efficiencies can be slightly overestimated in those cases having Ma $>$ 1 at the compressor rotor outlet. The high outlet Mach number can increase the compressor losses due to the presence of shock waves in the flow and can require special design considerations for impeller and diffuser flow passage shapes when compared to subsonic designs [48]. The high Mach number at the compressor outlet might also narrow the off-design operation range of the compressor as well as restrict the mass flow rate through the compressor in some conditions. If the losses related to the high Mach were recognized to be high in a more detailed compressor design analysis, such as in CFD analysis, the Mach number could be reduced by adjusting the compressor design specific speed, diameter ratios, or the shape of the velocity triangle (velocity ratios C_{u2}/U_2 and C_{r2}/U_2) in those design cases resulting otherwise in a high Mach number. However, in this study these compressor design parameters were kept as constant for all the studied fluids and conditions in order to compare the compressor sizes and preliminary loss estimations in a comprehensive way. For each

fluid combination the LT and HT compressor outlet Mach number corresponding to the heat pump design values with the maximum COP are presented in the *Appendix*.

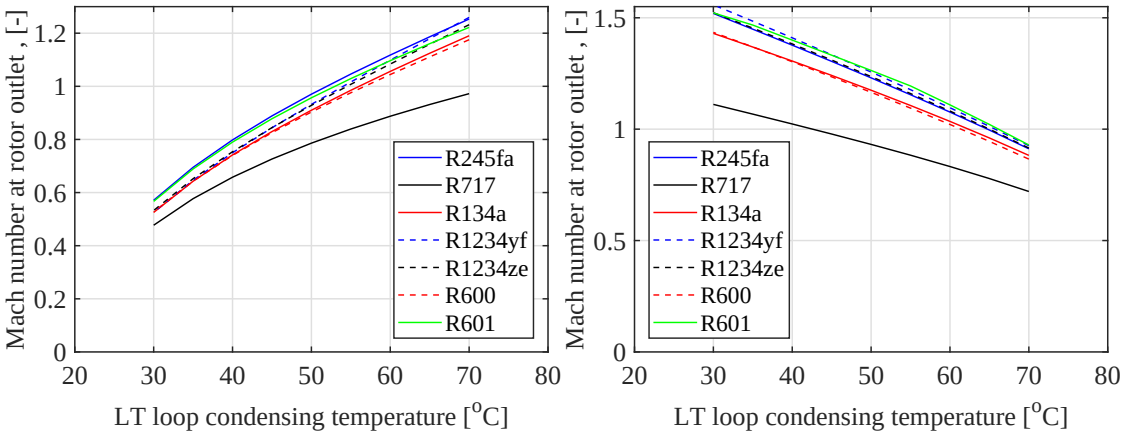

Figure 11: Effect of CHE temperature on Ma at rotor outlet. Figure (a) shows the LT compressor and (b) the HT compressor outlet Ma with different fluids.

4. Conclusions and discussions

The design and working fluid selection of a MW scale cascade heat pump capable of upgrading low grade waste heat was investigated with different fluids. It can be concluded, that the method of combining the thermodynamic analysis of the heat pump and the compressor design can provide an efficient tool for evaluating the different fluid combinations and design conditions, not only from the thermodynamic point of view but also based on the feasibility of centrifugal compressor design. The following conclusions and main observations were drawn.

1) The selection of working fluids and the temperature level in the cascade heat exchanger has a notable effect on the COP.

2) The fluid combinations with the highest performances reached COPs of over 3.0.

3) The highest performance of 3.08 was simulated using R601 in the low temperature cycle and R245fa in the high temperature cycle. High performances were also simulated with R601/R600, R601/R601, R245fa/R245fa, R600/R245fa and R245fa/R600.

4) The use of fluids with the lowest critical temperatures, namely R134a, R1234yf and R1234ze, showed the lowest performances, especially when these fluids were adopted in the high temperature cycle.

5) In general, maximum COP is reached when the temperature lift in the low temperature cycle is higher than the temperature lift in the high temperature cycle.

6) With R717 the maximum COP was lowered notably caused by low compressor efficiencies. This originated mainly from the small sized compressor and unfeasible high rotational speeds, as well as from the high tip clearance loss due to the low blade heights. Thus, R717 could be a more potential fluid candidate in large scale heat pumps. On the other hand, the use of R717 resulted in lower Mach numbers when compared to the other fluids.
7) Based on the compressor design analysis, the operational parameters and the different fluids have a significant impact on the compressor dimensions and optimal rotational speed. The use of fluids having a small enthalpy rise in the compressor and high mass flow rate results in lower compressor rotational speeds and larger sized compressor wheels when compared to the use of fluids with lower mass flow rate and higher enthalpy rise over the compressor.
8) The maximum COP is achieved in a design point that is not the point of highest efficiency of either the compressors, but instead it is a point where both of the compressors can be designed to operate with a reasonably high efficiency.
9) Tip clearance and skin friction loss make a significant contribution to the compressor losses according to the implemented loss correlations. In addition, leakage loss is a significant source of losses especially in those compressor designs that have low blade heights.
10) The speed of sound is low with the studied fluids resulting in supersonic flow conditions at the compressor wheel outlet when the compressor pressure ratio is high. This can increase the losses due to the presence of shock waves and requires special design considerations for the impeller and diffuser flow passages. If only subsonic impeller outlet velocities were considered the maximum COP of 2.91 is reached with the fluid combination R601/R1234ze.

It should be noted that despite the fact that the results of loss correlations and experimental data have shown relatively good agreement in previous studies for centrifugal compressors operating with refirgerants and other real gases, there can still be some uncertainties related to the accuracy of the loss models when different types of fluids are used as the correlations are mainly derived from experimental results for air driven centrifugal compressors. In addition, the effects of the low speed of sound of the fluids that can result in high Mach numbers at the rotor outlet might require additional design considerations and should be further investigated in the future. In addition, as the majority of the experimental activities on heat pump compressors have been carried out for rather small scale heat pump systems, the authors suggest that in the future it is important to carry out more experimental research with Megawatt scale centrifugal compressor driven heat pumps to further improve the efficiency predictions and loss correlations applicable for predicting the performance of large scale heat pump compressors. It should be highlighted, that in this paper the combined thermodynamic and compressor design analysis was used for investigating a large-scale cascade type heat pump but it is suggested that a similar method can be applied for investigating optimal

fluids and feasibility of the compressor design in heat pumps with different cycle layouts, temperature lifts and power scales.

References

[1] Johnson, I., Choate, W. T., and Davidson, A. (2008). Waste heat recovery. Technology and opportunities in US industry. BCS, Inc.

[2] Ebrahimi, K., Jones, G. F., and Fleischer, A. S. (2014). A review of data center cooling technology, operating conditions and the corresponding low-grade waste heat recovery opportunities. *Renewable and Sustainable Energy Reviews*, 31, 622-638.

[3] Chua, Kian J., Siaw K. Chou, and W. M. Yang. (2010). Advances in heat pump systems: A review. *Applied energy* 87, no. 12: 3611-3624.

[4] Arpagaus, C., Bless, F., Uhlmann, M., Schiffmann, J., and Bertsch, S. S. (2018). High temperature heat pumps: Market overview, state of the art, research status, refrigerants, and application potentials. *Energy*, 152, 985-1010.

[5] Averfalk, H., Ingvarsson, P., Persson, U., Gong, M., and Werner, S. (2017). Large heat pumps in Swedish district heating systems. *Renewable and Sustainable Energy Reviews*, 79, 1275-1284.

[6] Riipinen, M. (2013). District heating and cooling in Helsinki. In International Energy Agency CHP/DHC Collaborative and Clean Energy.

[7] Urbanucci, L., Bruno, J. C., and Testi, D. (2019). Thermodynamic and economic analysis of the integration of high-temperature heat pumps in trigeneration systems. *Applied energy*, 238, 516-533.

[8] Calm, J. M., and Hourahan, G. C. (2011). Physical, safety, and environmental data for current and alternative refrigerants. In Proceedings of 23rd International Congress of Refrigeration, Prague, August (pp. 21-26).

[9] Reissner F. (2015) Development of a Novel High Temperature Heat Pump System, Entwicklung eines neuartigen Hochtemperatur-Wrmepumpensystems. PhD Thesis. Friedrich-Alexander Universitat Erlangen-Nurnberg.

[10] Zhang J, Zhang H-H, He Y-L, Tao W-Q. (2016) A comprehensive review on advances and applications of industrial heat pumps based on the practices in China. *Applied Energy* 178:80025.

[11] Domanski, P.A., Brown, J.S., Heo, J., Wojtusiak, J., and McLinden, M. O. (2014). A thermodynamic analysis of refrigerants: Performance limits of the vapor compression cycle. *International Journal of Refrigeration*, 38, 71-79.

[12] Zhang, S., Wang, H., and Guo, T. (2010). Experimental investigation of moderately high temperature water source heat pump with non-azeotropic refrigerant mixtures. *Applied Energy*, 87(5), 1554-1561.

[13] Fukuda, S., Kondou, C., Takata, N., and Koyama, S. (2014). Low GWP refrigerants R1234ze (E) and R1234ze (Z) for high temperature heat pumps. *International journal of Refrigeration*, 40, 161-173.

[14] Wang W, Ma Z, Jiang Y, Yang Y, Xu S, Yang Z. (2005) Field test investigation of a double-stage coupled heat pumps heating system for cold regions. *International Journal of Refrigeration*, 28(5):6729.

[15] Kim, D. H., Park, H. S., and Kim, M. S. (2013). Optimal temperature between high and low stage cycles for R134a/R410A cascade heat pump based water heater system. *Experimental thermal and fluid science*, 47, 172-179.

[16] Ma, X., Yufeng Z., Xiaoqiong L., Hongfu Z., Na D., Jinzhe N. et al. (2018). Experimental study for a high efficiency cascade heat pump water heater system using a new near-zeotropic refrigerant mixture. *Applied Thermal Engineering*, 138: 783-794.

[17] Kim, D. H., and Kim, M. S. (2014). The effect of water temperature lift on the performance of cascade heat pump system. *Applied thermal engineering*, 67(1-2), 273-282.

[18] Messineo A. and Panno D. (2012) Performance evaluation of cascade refrigeration systems using different refrigerants, *International Journal of Air-Conditioniong and Refrigeration*. vol.20 1250010

[19] Winandy, E., Saavedra, C., and Lebrun, J. (2002). Experimental analysis and simplified modelling of a hermetic scroll refrigeration compressor. *Applied thermal engineering*, 22(2), 107-120.

[20] Huagen, W., Ziwen, X., and Pengcheng, S. (2004). Theoretical and experimental study on indicator diagram of twin screw refrigeration compressor. *International Journal of Refrigeration*, 27(4), 331-338.

[21] Bamigbetan, O., Eikevik, T. M., Nekså, P., Bantle, M., and Schlemminger, C. (2019). Experimental investigation of a prototype R-600 compressor for high temperature heat pump. *Energy*, 169, 730-738.

[22] Friotherm AG. Uniturbo22 Centrifugal Compressor for large scale refrigeration plants and heat pumps, G00105. 2017. www.friotherm.com.

[23] Schiffmann, J., and Favrat, D. (2009). Experimental investigation of a direct driven radial compressor for domestic heat pumps. *International Journal of Refrigeration*, 32(8), 1918-1928.

[24] Schiffman J., and Favrat D. (2010) Design, experimental investigation and multi-objective optimization of a small-scale radial compressor for heat pump applications. *Energy.* 35, 436-450

[25] Meroni, A., Zuhlsdorf, B., Elmegaard, B., and Haglind, F. (2018). Design of centrifugal compressors for heat pump systems. *Applied energy*, 232, 139-156.

[26] Turunen-Saaresti, T., Röyttä, P., Honkatukia, J., and Backman, J. (2010). Predicting off-design range and performance of refrigeration cycle with two-stage centrifugal compressor and flash intercooler. *International journal of refrigeration*, 33(6), 1152-1160.

[27] Röyttä, P., Turunen-Saaresti, T., and Honkatukia, J. (2009). Optimising the refrigeration cycle with a two-stage centrifugal compressor and a flash intercooler. *International Journal of Refrigeration*, 32(6), 1366-1375.

[28] Lemmon, E. W., Huber, M. L., and McLinden, M. O. (2010). NIST Standard Reference Database 23, NIST Reference Fluid Thermodynamic and Transport Properties, REFPROP, version 9.0. Standard Reference Data Program.

[29] Gong, M., and Werner, S. (2015). Exergy analysis of network temperature levels in Swedish and Danish district heating systems. *Renewable energy*, 84, 106-113.

[30] Lund, H., Werner, S., Wiltshire, R., Svendsen, S., Thorsen, J. E., Hvelplund, F., et al. (2014). 4th Generation District Heating (4GDH): Integrating smart thermal grids into future sustainable energy systems. *Energy*, 68, 1-11.

[31] Uzhegov, N., Kurvinen, E., Nerg, J., Pyrhonen, J., Sopanen, J., Shirinskii, S., (2016). Multidisciplinary Design Process of a 6-Slot 2-Pole High-Speed Permanent Magnet Synchronous Machine. *IEEE Transaction on Industrial Electronics*, 63(2), 784-795.

[32] Wang, G., Chen, Z., Li, C., and Jiang, B. (2017). Preliminary theoretical analyses of thermal performance and available energy consumption of two-stage cascade cycle heat pump water heater. *International Journal of Refrigeration*, 82, 381-388.

[33] Japikse, D. (1996). Centrifugal compressor design and performance. Concepts ETI, Inc. ISBN 0-933283-03-2

[34] Balje, O.E. (1980). Turbomachines: A Guide to Design, Selection, and Theory. Wiley,New York.

[35] Came, P.M., and Robinson, C.J. (1999). Centrifugal compressor design. Proceedings of the Institution of Mechanical Engineers, Part C: *Journal of Mechanical Engineering Science*, 213(2), 139-155.

[36] Oh, H.W., Yoon, E.S., and Chung, M.K. (1997). An optimum set of loss models for performance prediction of centrifugal compressors.*Journal of Power and Energy*, 211(4), 331-338.

[37] Lee, J., Lee, J. I., Yoon, H. J., and Cha, J. E. (2014). Supercritical Carbon Dioxide turbomachinery design for water-cooled Small Modular Reactor application. *Nuclear Engineering and Design*, 270, 76-89.

[38] Ameli, A., Afzalifar, A., Turunen-Saaresti, T., and Backman, J. (2019). Centrifugal Compressor Design for Near-Critical Point Applications. *Journal of Engineering for Gas Turbines and Power*, 141(3), 031016.

[39] Daily, J.W. and Nece, R.E. (1960). Chamber dimension effects on induced flow and frictional resistance of enclosed rotating disks. *Journal of Basic Engineering* 82, 217232.

[40] Jansen, W. (1967). A method for calculating the flow in a centrifugal impeller when entropy gradients are present. Royal Society Conference on Internal Aerodynamics (Turbomachinery), pp. 133146.

[41] Coppage, J.E., and Dallenbach, F. (1956). Study of supersonic radial compressors for refrigeration and pressurization systems, WADC Report 55-257.

[42] Aungier, R.H. (1995). Mean streamline aerodynamic performance analysis of centrifugal compressors. Transactions of the ASME *Journal of Turbomachinery*, 117, 360366.

[43] Oh, H.W., Chung, M.K (1999). Investigation on the Design and Performance Analysis Methods of Centrifugal Turbomachines. KAIST.(Doctoral thesis)

[44] Johnston, J.P., and Dean Jr., R.C. (1966). Losses in vaneless diffusers of centrifugal compressors and pumps. Analysis, experiment, and design. *Journal of Engineering for Power*, 88, 4962.

[45] Uusitalo A., Ameli A., and Turunen-Saaresti T. (2019) Thermodynamic and turbomachinery design analysis of supercritical Brayton cycles for exhaust gas heat recovery. *Energy*, 167. 60-79

[46] Naukkarinen T. (2013) The Aerodynamic Design of A Centrifugal Compressor. Master Thesis, Lappeenranta University of Technology (In Finnish)

[47] Dewar, B., Tiainen, J., Jaatinen-Värri, A., Creamer, M., Dotcheva, M., Radulovic, J., et al. (2019). CFD modelling of a centrifugal compressor with experimental validation through radial diffuser static pressure measurement. *International Journal of Rotating Machinery*.

[48] Larjola J. (1988). Centrifugal compressors, the fundamentals of design, Lappeenranta university of technology, publ no. No EN B-61 (In Finnish)

Appendix

Table A1: LT cycle condensing temperature [°C], LT cycle pressure ratio [-] and HT cycle pressure ratio [-] corresponding to the design values with maximum COP.

	R245fa	R717	R134a	R1234yf	R1234ze	R600	R601
R245fa	60/3.77/2.92	55/2.70/3.42	55/2.61/3.42	55/2.48/3.42	55/2.65/3.42	60/3.07/2.92	65/4.37/2.51
R717	65/4.34/2.21	60/3.05/2.52	60/2.94/2.52	65/2.48/2.87	60/2.99/2.52	65/3.47/2.21	70/5.01/1.96
R134a	70/4.97/1.93	65/3.44/2.18	65/3.31/2.18	60/2.77/2.46	65/3.36/2.18	70/3.90/1.93	70/5.01/1.93
R1234yf	70/4.97/1.88	70/3.86/1.88	65/3.31/2.10	65/3.10/2.10	70/3.77/1.88	70/3.90/1.88	70/5.01/1.88
R1234ze	70/5.01/1.94	65/3.90/1.94	60/3.36/2.19	60/2.77/2.48	60/2.94/2.48	70/3.44/2.19	70/4.97/1.94
R600	60/3.77/2.52	55/3.05/2.52	55/2.61/2.88	55/2.48/2.88	55/2.65/2.88	60/3.07/2.52	65/4.37/2.22
R601	60/4.34/2.86	55/3.44/2.86	60/2.94/3.46	55/2.48/4.20	55/2.99/3.46	65/3.47/2.86	65/5.01/2.39

Table A2: Total compressor power consumption [kW], LT compressor efficiency [%] and HT compressor efficiency [%] corresponding to the design values with maximum COP.

	R245fa	R717	R134a	R1234yf	R1234ze	R600	R601
R245fa	470/84/83	505/74/83	497/81/83	507/82/83	493/82/83	474/83/83	459/84/83
R717	505/83/72	544/73/71	539/81/71	549/81/72	534/82/71	510/82/72	492/84/73
R134a	529/82/82	574/72/81	574/80/81	590/82/81	568/81/81	535/81/82	513/84/81
R1234yf	559/82/83	606/70/83	614/80/82	639/81/82	606/80/83	565/81/83	542/84/83
R1234ze	514/82/82	557/72/82	555/81/81	571/82/81	550/82/81	520/81/82	498/84/82
R600	476/84/82	512/74/81	504/81/81	514/82/81	500/82/81	480/83/82	465/84/82
R601	490/84/84	531/74/83	526/81/84	541/82/83	521/82/83	495/82/84	475/84/84

Table A3: Rotational speed of the LT and HT compressor [krpm] corresponding to the design values with maximum COP.

	R245fa	R717	R134a	R1234yf	R1234ze	R600	R601
R245fa	14.8/17.6	148.0/17.8	20.5/17.8	20.4/17.8	20.6/17.8	28.6/17.6	17.7/17.0
R717	15.5/166.1	161.3/176.7	26.6/177.0	20.4/187.4	21.7/177.2	30.2/166.1	18.5/152.4
R134a	16.2/23.0	173.6/24.4	27.8/24.4	21.4/25.7	22.6/24.4	31.4/22.9	18.6/23.1
R1234yf	16.2/17.3	184.9/17.0	27.8/18.2	22.0/18.1	23.3/17.0	31.4/17.2	18.5/17.3
R1234ze	16.2/19.6	173.6/20.7	26.6/21.8	21.4/21.7	22.6/20.7	31.4/19.6	18.5/19.7
R600	14.8/31.9	161.3/31.5	25.1/32.7	20.4/32.6	20.6/32.7	28.6/31.9	17.7/30.5
R601	15.5/20.7	173.6/20.5	26.6/21.1	20.4/21.4	21.7/21.1	30.2/20.7	18.5/19.8

Table A4: Outlet diameter of the LT and HT compressor [mm] corresponding to the design values with maximum COP.

	R245fa	R717	R134a	R1234yf	R1234ze	R600	R601
R245fa	272/207	71/219	150/219	165/219	175/218	195/207	331/199
R717	272/57	70/58	150/58	165/59	176/58	196/57	332/56
R134a	275/130	69/134	152/134	167/138	178/134	197/130	332/129
R1234yf	275/153	69/155	152/159	171/160	181/155	197/153	332/152
R1234ze	275/146	69/152	150/156	167/157	178/151	197/147	332/146
R600	272/160	70/162	150/167	165/168	175/167	195/160	331/155
R601	272/245	69/248	150/261	165/278	176/261	196/245	332/234

Table A5: Mach number at the rotor outlet of the LT and HT compressor corresponding to the design values with maximum COP.

	R245fa	R717	R134a	R1234yf	R1234ze	R600	R601
R245fa	1.11/1.08	0.84/1.15	0.99/1.15	1.02/1.15	1.01/1.15	1.04/1.08	1.16/1.00
R717	1.22/0.72	1.11/0.78	1.08/0.83	1.02/0.88	1.06/0.83	0.89/0.83	1.19/0.79
R134a	1.25/0.88	0.93/0.96	1.12/0.96	1.10/1.03	1.16/0.96	1.17/0.88	1.22/0.88
R1234yf	1.25/0.93	0.97/0.93	1.12/1.01	1.17/1.01	1.23/0.93	1.18/0.93	1.22/0.93
R1234ze	1.25/0.92	0.93/1.00	1.06/1.08	1.10/1.08	1.16/1.00	1.17/0.92	1.22/0.92
R600	1.11/1.02	0.89/1.02	0.99/1.09	1.02/1.09	1.01/1.09	1.04/1.02	1.16/0.95
R601	1.18/1.02	0.93/1.02	1.06/1.11	1.02/1.19	1.08/1.11	1.11/1.02	1.22/0.93